

Energy Resource Allocation for Green FiWi Network using Ensemble Learning

Akshita Gupta¹, Halwai Sakshi Gupta², Vivek Ashok Bohara¹, and Anand Srivastava¹

¹Wirocomm Research Group, Department of Electronics & Communication Engineering, Indraprastha Institute of Information Technology Delhi (IIITD), New Delhi, 110020, India.

²Cochin University of Science and Technology, University in Kochi, Kerala

Email: akshitag@iiitd.ac.in, sakshi81818@gmail.com, vivek.b@iiitd.ac.in, anand@iiitd.ac.in

Abstract—In this paper, we utilize a random forest regression based ensemble learning to effectively predict the solar power available for the fiber-wireless (FiWi) network components, such as optical network units (ONUs) and access points (APs) which is collectively known ONU-AP. Thereafter, a joint energy resource allocation framework is proposed to minimize the required number of photovoltaic (PV) panels and batteries. To solve the joint energy resource allocation problem, we divide it into two sub-problems, minimum PV panel allocation for a fixed number of batteries and minimum battery allocation for a fixed number of PV panels. The two sub-problems are further solved using the proposed *MinBatAlloc* and *MinPVAlloc* algorithms. Moreover, we introduce a system parameter α , that signifies the ratio between solar power supplied to operate ONU-AP and to charge the batteries. The results are shown by varying α and its impact on the energy resource allocation and battery lifetime. We compare the performance of our proposed approach with non-ML based approaches, such as, maximum, minimum, median, and outage threshold based energy resource allocation. Through the obtained results it has been shown that the proposed approach considerably improves the performance in terms of outage, lifetime, carbon dioxide emissions, and cost.

Index Terms—Fiber-wireless (FiWi), Joint energy resource allocation, Wind turbine, Lifetime, Cost-analysis, Carbon dioxide (CO₂) emissions.

I. INTRODUCTION

Green access network, i.e., energy-efficient access network has been a focus of recent literature as it reduces the dependency on non-renewable sources of energy and also facilitate the path to a sustainable future. Moreover, it also alleviates the reliance on intermittent grid power supply while reducing the carbon footprint [1]. In 2021, the electricity generation from renewable sources is expected to be 8300 TWh, with the major electricity generation in China, followed by United States, European Union, and India [2]. Further, the electricity generation from solar and wind panels is expected to cover about two-thirds of the renewable electricity market [2].

The information and communications technology (ICT) sector is expected to have a yearly growth rate of 5% from 2021-2023 [3]. The carbon emissions from ICT is estimated to increase by 1.4% in 2021 [4]. The carbon-dioxide (CO₂) emissions is going to increase further as the demand for ubiquitous and uninterrupted coverage increases. However, the above can be alleviated by usage of green sources such as wind

and solar energy. One of the major limitations of green sources is their intermittent availability and variation depending on the location. As a consequence, depending on the location and utilization, it is important to plan the energy resource allocation so as to ensure that the green resources are neither under-utilized nor over-utilized.

A. Related Works

Fiber-wireless (FiWi) network combines the advantages of fiber backhaul network with wireless fronthaul. FiWi network consists of passive optical network (PON) as the backhaul network with wireless network such as, wireless fidelity (WiFi), wireless local area network (WLAN), etc. as the fronthaul [10], [11]. As these networks need to be operated round the clock, therefore it is imperative to allocate energy resources to the network such that the network is cost efficient. In [12], the authors have proposed a frame aggregation for Internet of things (IoT) over FiWi network. The authors used load transfer along with frame aggregation to reduce the energy consumption of the FiWi network. Depending on the channel quality, the length of the aggregated frame is computed. Further, in order to maximize the sleep duration of optical network unit (ONU), the traffic is prioritized based on the delay requirement of voice and video traffic. This in turn, reduces the retransmission of packets due to poor channel quality, and thus, reduces the excessive energy consumption of the network. The authors in [13] proposed an iterative search algorithm for energy-aware collaborative computation offloading. The proposed algorithm not only increases the battery lifetime of the smart mobile devices but also increases the energy efficiency of the backhaul network. However, [12], [13] do not consider any renewable sources of energy to power the FiWi network components. In [14], the authors proposed a 5G new radio (NR) based FiWi network which is powered by means of a power over fiber system. Specifically, it operates a low-power 5G NR remote antenna unit, composed of a photodetector and radio-frequency (RF) amplifier, by means of a power over fiber system. The authors were able to achieve a power transmission efficiency of 23.5%. A two layer Stackelberg game based offloading scheme is proposed in [15] to allocate the channel bandwidth as well as to make offloading decisions. Further,

TABLE I
SUMMARY OF RELATED WORKS ON SOLAR PREDICTION

Reference	Algorithm used	Contributions
[5]	Markov Chain model	Forecasted solar irradiance by investigating the use of the Markov chain model for a short-term period
[6]	Markov switching model	Markov regime switching model performs better than solar radiance forecasting models, such as the persistence model, neural network, GPR, and auto regression model
[7]	Artificial NN	Artificial NN model to produce solar power forecasts compared to linear regression and persistence models
[8]	Combination of KBNN and MLP	Proposed model had a 64.5% more accuracy compared to existing models
[9]	Long Short-Term Memory	Used local weather forecast and a pretrained LSTM model to predict next-day solar irradiance

the authors also proposed energy efficiency benchmarks from both system-wide and user-side perspectives. However, the authors modified the standard energy consumption protocol to conserve the energy and did not use any renewable sources of energy to operate the network components. In [1], the authors used a combination of renewable energy sources such as solar as well as other non-renewable sources such as batteries for FiWi network. Specifically, an energy resource allocation approach to operate ONU is proposed for on-grid as well as off-grid scenarios¹. However, they did not use any ML based energy resource allocation to allocate the energy resources dynamically based on the availability of solar power. In [16], the authors formulated a two-stage photovoltaic (PV) planning framework for distribution grids using a game theory approach. First, the authors computed the optimal installation capacity of PV panels, then they proposed a model to optimally allocate PV panels among the solar producers and consumers to minimize the active power flow in the system. However, the authors did not use any other renewable source such as wind, nor did they employ any ML based technique for allocating the PV panels. The authors in [17] used a cooperative game theory scheme to investigate the performance of shared PV panel system among community of households. In [18], a power allocation scheme for battery cluster switching is proposed to alleviate overcharging and deep-charging of batteries as well as to minimize the battery power loss. However, the authors did not consider solar and wind energy. The authors in [19] developed a novel statistical model of the harvested energy from renewable energy sources considering harvest-store-consume (HSC) architecture. They derived the closed-form expressions for the density functions and moments of the harvested solar and wind power using clouds occlusion, wind speed, etc. Further, in [20], the authors reviewed the performance of miniaturized wind energy harvesters (MWEHs). A miniature wind energy harvester design which works at low wind speed with a wide operational wind speed range can significantly improve the operation cycle of many systems and can result in more robust Internet of Things (IoT) applications. However, in order to capture the day-to-day fluctuation in wind

and solar power, the practical values for parameters such as cloud occlusion are required. Moreover, unlike solar power, the wind power do not follow any specific hourly pattern. Thus, it is difficult to consider any specific statistical model for wind power.

The accurate predictions about the availability of the green sources of energy will facilitate to quantify their future availability. In [5], the authors proposed the Markov Chain model to forecast the hourly day-ahead solar irradiance for Jodhpur, India. The authors achieved a maximum solar irradiance root mean square error (RMSE) of 2200.818 W/m² for October 2014 and maximum mean absolute error (MAE) of 90.985 W/m² for July 2014. A typical Markov chain model to quantify the solar prediction for bi-hourly data is proposed in [6]. The performance in terms of mean square error (MSE), MAE, RMSE, standard deviation error (SDE) is compared with four types of prediction model, namely, persistent, autoregressive, Gaussian process regression (GPR) model, and neural network (NN) [6]. The results demonstrated that using Markov switching, the authors were able to get the best performance, followed by NN, whereas the performance of GPR is the worst. Using artificial NN (ANN), the authors in [7] compared the performance of hourly solar power forecasting with multiple layer regression and persistence method. The authors showed that depending on the weather conditions, the forecast might vary. For instance, clear sky hours have better forecast compared to cloudy hours. The authors in [8] proposed a model composed of knowledge based NN (KBNN) and multilayer perceptron (MLP) for forecasting solar power. The results demonstrated that the model is reliable even when the training data is insufficient. Moreover, the model is shown to have an accuracy improvement of 65.4% compared to existing methods. In [9], the authors used long short-term memory (LSTM) model for solar energy prediction for Korea. The authors used weather forecast statistics such as temperature, sky cover, humidity, etc., to forecast solar irradiance. Moreover, they showed that the LSTM model had the RMSE coefficient of 12%. Table I summarizes the related works on solar power predictions.

¹The scenarios where grid energy is utilized to power the network components are called on-grid scenario, whereas the scenarios where grid energy is not utilized are called off-grid scenarios.

B. Contributions

Motivated by the above, we propose a machine learning (ML) based joint energy resource allocation framework to allocate batteries and photovoltaic (PV) panels for an off-grid green FiWi network. As the solar power profile generally differs for each day, thus energy resource allocation needs to be done such that the resources are neither under-utilized nor over-utilized. In order to allocate the energy resources at any specific location, it is essential to predict the solar power at that location. The existing resource allocation algorithms do not take into account the dynamic nature of energy resource allocation based on day-to-day solar power availability. In order to do so, we propose an ML based energy resource allocation framework wherein for predicting the solar power we have used random forest based ensemble learning. The FiWi network consists of 10-Gigabit-capable passive optical network (XG-PON) with WiFi frontend. The ONU and access point (AP) are co-located and are collectively called ONU-AP [21]. The ONU-AP is powered using solar and wind energy along with batteries. In order to allocate the PV panels and batteries to operate ONU-AP, a joint energy resource allocation problem is formulated. The joint energy resource allocation problem is divided into two sub-problems. These sub-problems are then solved alternatively to find the required minimum energy resource allocation. This paper compares the proposed ML based energy resource allocation (*MERA*) approach with the traditional approach such as a) *Max* energy resource allocation, b) *Min* energy resource allocation, c) *Median* energy resource requirement, and d) Outage threshold based energy resource allocation.

Some of the major contributions of the proposed work are summarized as follows:

- We introduce a system parameter α , that indicates the ratio between the solar power supplied to operate ONU-AP and the solar power supplied to charge the batteries. The results are shown by varying α and its impact on the energy resource allocation and battery lifetime.
- Based on the solar power available to ONU-AP, we propose a joint optimization framework to minimize the number of batteries and PV panels required to operate ONU-AP for an off-grid scenario, where ONU-AP is powered using solar power, wind power, and batteries.
- To solve the non-linear joint optimization problem, we divide it into two sub-problems: 1) Minimum PV panel allocation for a fixed number of batteries and 2) Minimum battery allocation for a fixed number of PV panels. Each sub-problem is then solved using proposed algorithms: a) *MinPVAlloc*: to calculate the minimum PV panel allocation for a fixed number of batteries and b) *MinBatAlloc*: to calculate the minimum battery allocation for a fixed number of PV panels. These algorithms are then solved alternatively to find the optimal energy resource allocation for ONU-AP.
- We propose ML based energy resource allocation approach (*MERA*) that uses hourly solar irradiance forecast

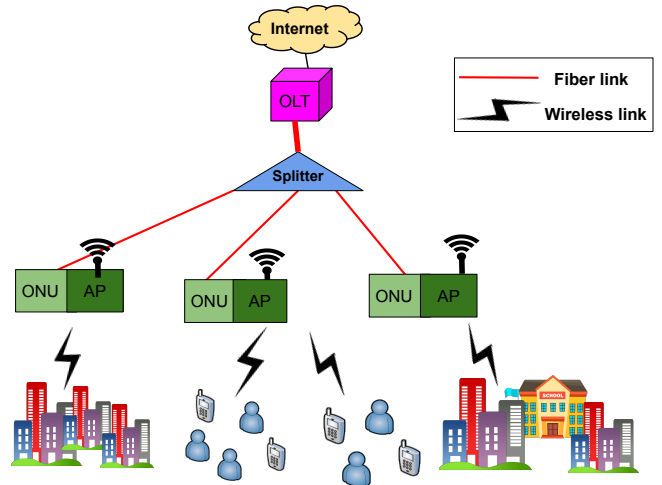


Fig. 1. System architecture for FiWi network

to dynamically allocate the energy resource required to operate ONU-AP. In order to forecast the solar irradiance profile, we use random forest based ensemble learning.

- We compare the performance of proposed approach, *MERA* with the traditional approaches such as a) *Max* energy resource allocation, b) *Min* energy resource allocation, c) *Median* energy resource requirement, and d) Outage threshold based energy resource allocation. Further, we analyze the performance of *MERA* with the traditional approaches in terms of battery lifetime, outage, CO₂ emissions, and cost.

The results demonstrate that with the usage of *MERA*, the system performance in terms of outage, cost, and CO₂ emissions improves. Specifically, due to dynamic resource allocation, we are able to get an outage performance lower than the *Max* energy resource allocation, which is the based on the worst 24-hour solar power profile of the year. Moreover, there is also a reduction in cost and CO₂ emissions using *MERA* as compared to *Max* approach. Furthermore, it is shown that with the usage of green energy sources, the CO₂ emissions have also significantly reduced by 3.8 metric tonnes compared to traditional grid power supply over a period of one year.

The rest of the paper is organized as follows. Section II presents the system model for the proposed FiWi network. The solar irradiance prediction model is presented in Section III. The joint optimization problem formulation is discussed in Section IV. The proposed framework for joint energy resource allocation is presented in Section V. The performance of proposed approach is evaluated in Section VI. Finally, Section VII concludes the paper.

Notations: The vector is denoted as boldface as \mathbf{x} . The set of positive real integers is denoted by \mathbb{Z} .

II. SYSTEM MODEL

In this section, we discuss the system model and related parameters for the considered green FiWi network.

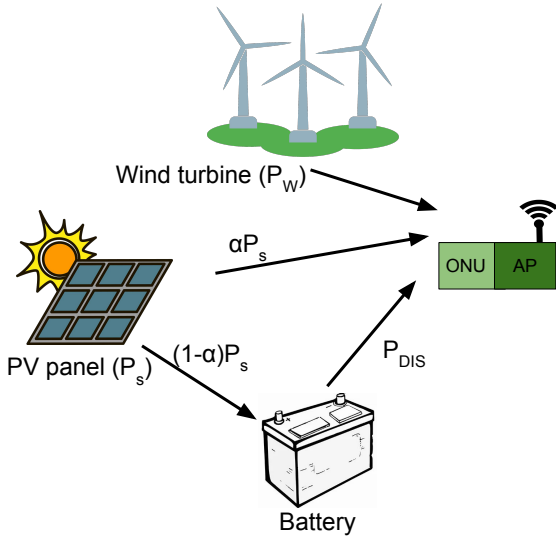


Fig. 2. Power supply model of ONU-AP.

A. Network Model

The system model for the considered FiWi network is shown in Fig. 1. We consider a FiWi network consisting of an XG-PON as the backhaul network and WiFi as the fronthaul network. XG-PON network consists of an optical line terminal (OLT) at the central office. During uplink communication, the user sends data to AP which further sends it to ONU. The ONU and AP are co-located and are commonly known as ONU-AP [21]. The traffic from the ONUs is then combined using a passive splitter and sent to the OLT. The ONU-AP is powered using solar panels, batteries, and wind turbines as evident from Fig. 2. It is assumed that the solar panels along with powering ONU-APs are also responsible for charging the batteries whereas the wind turbines are only used to power ONU-APs. This is due to the fact that wind power is generally erratic and therefore, it is not used to power the battery. In Fig. 2, it can be seen that P_S is the solar power generated by ONU-AP. α is the fraction of solar power supplied to ONU-AP, i.e., the solar power supplied to ONU-AP is denoted as αP_S , where $0 \leq \alpha \leq 1$. The remaining fraction of solar power, $(1 - \alpha)P_S$ is supplied to the batteries. P_{DIS} is the power supplied by the batteries to power ONU-AP. The batteries power ONU-AP for operation during non-solar hours or the hours where the available solar power is less than the power requirement of ONU-AP.

B. Throughput Model

Depending on the time of the day, the density of the users also varies, for instance, the density of users is high during the peak traffic hours and low during the night hours. In [22], the authors provided statistical modelling of time varying throughput per cell and the distribution of instantaneous throughput per cell over different cells based on throughput measurements from a real-world large-scale urban cellular network. The throughput profile for the users follows an

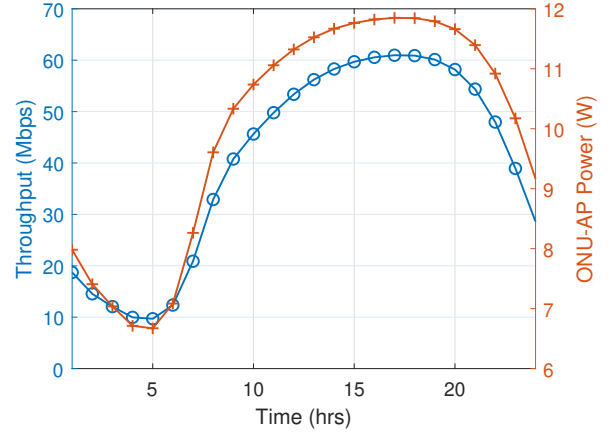


Fig. 3. Throughput and power consumption profile of ONU-AP.

exponential probability density function with rate parameter, r given by Gaussian mixture model (GMM) as [22]:

$$r = \sum_{i=1}^k a_i e^{-\left(\frac{t-\Delta_i}{\lambda_i}\right)^2}, \quad (1)$$

where a_i is the amplitude of the i^{th} peak, t is the time (in hours) of the day, λ_i relates to the peak width of the i^{th} peak, $k = 7$ represents the number of peaks in the data series, and Δ_i is the location of the centroid of the i^{th} peak [22]. The curve fitting parameters have the values as: $\mathbf{a} = [3.263 \times 10^6, 0.0781, 0.6616, 0.1097, 0.2584, 0.1822, 0.1652]$, $\mathbf{\Delta} = [75.273, 3.85, 4.971, 2.996, 1.868, 3.221, -2.871]$, and $\mathbf{\lambda} = [12.56, 0.4829, 1.77, 0.862, 1.543, 5.972, 84]$ [22].

The aggregated throughput profile of all the users connected to ONU-AP is shown in Fig. 3 [1]. It is evident that at night (3:00-7:00 hrs), as the number of users accessing the network is low, the throughput of the network is also low, whereas for the peak traffic hours (17:00-19:00 hrs), a peak in the throughput profile can be observed.

C. Power Consumption Model of ONU-AP

The power consumption profile for ONU-AP is presented in this subsection. The sum of the power consumption of ONU and AP is the power consumption of ONU-AP. Further, the power consumption of the network devices depends on the throughput profile of the network. Fig. 3 shows the throughput as well as power consumption profile of ONU-AP. Depending on the state of ONU, the power consumption of ONU varies. According to [23], ONU can be in the following states:

- 1) *Active held state*: In this state ONU is awake and consumes full power.
- 2) *Asleep state*: In this state both transmitter and receiver of ONU are turned off.
- 3) *Sleep aware state*: In this state ONU checks whether there is any traffic in the network or whether it can go to asleep state.

- 4) *Active free state*: The ONU at this stage decides whether it can go to a low power consumption state based on the downstream traffic.
- 5) *Listen state*: In this state the transmitter is off but the receiver is on.

The power consumption model for wireless IEEE 802.11 devices also depends on upstream and downstream data rate, i.e., δ_u and δ_d , respectively. The power consumption for IEEE WiFi APs is shown in [24]. Let, P_{as} , P_{ah} , P_{da} , P_{ls} , P_{sa} , and P_{af} be the power consumption of different states of ONU denoted as active free, doze aware, listen, asleep, sleep aware, and active held, respectively. The power consumption of ONU-AP is given as [23] [24]:

$$\begin{aligned}
P_{ONU-AP} = & \gamma_{sa}P_{sa} + \gamma_{as}P_{as} + \gamma_{ah}P_{ah} \\
& + \gamma_{da}P_{da} + \gamma_{ls}P_{ls} + \gamma_{af}P_{af} + P_{idle} \\
& + P_{Tx}T_{Tx} + P_{Rx}T_{Rx} + \gamma_{gx}\delta_d + \gamma_{xr}\delta_u, \quad (2)
\end{aligned}$$

where γ_{as} , γ_{ah} , γ_{da} , γ_{ls} , γ_{sa} , and γ_{af} are the stationary probabilities for each state. Moreover, $\gamma_{sa} + \gamma_{as} + \gamma_{ah} + \gamma_{da} + \gamma_{ls} + \gamma_{af} = 1$. T_{af} , T_{da} , T_{ls} , T_{as} , T_{sa} , and T_{ah} are the time periods of active free, doze aware, listen, asleep, sleep aware, and active held states of ONU, respectively. P_{idle} is the power consumption of AP in the idle mode, P_{Rx} and P_{Tx} are the reception and transmission power, respectively. T_{Tx} and T_{Rx} is the transmission and reception airtime percentage, the reception cross-factor is given by γ_{xr} , and the cross-factor of the packets generated by the application is denoted by γ_{gx} . In this paper, we consider $\delta_u = \delta_d$, i.e., symmetric data rate scenario for upstream and downstream scenario [25], [26]. The burst size for the traffic is considered to be 450 bytes [1]. The values of $P_{Rx} = 0.24 W$, $P_{idle} = 3.68 W$, $P_{Tx} = 0.4 W$, and $\gamma_{xr} = \gamma_{gx} = 0.93 \times 10^{-3}$ [24], and $T_{Rx} = T_{Tx} = 50\%$ [27].

D. Solar Power Model

The solar irradiance profile for different cities can be obtained from National Renewable Energy Laboratory (NREL) [28]. The solar irradiance is then converted to the solar power profile as follows [29]:

$$P_S = I\eta A \frac{T_c}{100}(T_o - 25), \quad (3)$$

where I is the irradiance profile discussed later, $\eta = 20.55\%$ is the efficiency of solar panel, A is the area of the solar panel, $T_c = -1.039$ is the temperature coefficient, T_o is the temperature [29].

E. Wind Power Model

The speed of the wind depends on the location of installation and the wind turbine's height. Based on the air density and wind speed, the wind power generated by the wind turbine is given by [30]:

$$P_W = 0.5\rho\pi R^2 v_w^2 C_{pmax}, \quad (4)$$

where R is blade radius of wind machine, ρ is air density, C_{pmax} is the maximum rotor power coefficient, and v_w is wind speed. For simulations, we consider a 50 m height of

the wind turbine, $R = 0.5$ m, $\rho = 1.225$ kg/m³, and $C_{pmax} = 0.042$ [31].

F. Battery Model

Batteries are one of the main energy sources required to power the network components when the grid power supply and renewable energy sources are not available. Lead-acid batteries are cost-effective and are one of the popular types of batteries [32]. Moreover, unlike other batteries sources, the partial state of charge (SoC) has minimal effect on the lifetime of the lead-acid batteries [32]. Let us assume the capacity for each battery is P_{Bcap} . The state of charge of the battery is updated whenever the batteries are discharged or charged. If the SoC of the batteries reaches P_{Bcap} , the batteries cannot be charged further. Further, a depth of discharge (DoD) value is generally predefined by the operators that specifies the battery's minimum state of charge. The battery lifetime can be enhanced by maintaining the DoD, i.e., avoid deep discharge. In this paper, a series configuration of batteries is considered; thus, if we consider a deployment of N batteries with battery capacity P_{Bcap} then, the overall capacity of the N batteries will be NP_{Bcap} [1].

III. SOLAR IRRADIANCE PREDICTION USING ML

This section of the paper focuses on predicting global horizontal irradiance (GHI). GHI is defined as the total solar radiation incident on a horizontal surface and is used in (3). This can be calculated by using [29] as

$$I = D_N \cos(\theta) + D_H, \quad (5)$$

where, D_N is direct normal irradiation (DNI) and is defined as the amount of solar radiation received per unit area by a surface that is held perpendicular (or normal) to the rays and D_H is diffuse horizontal irradiance (DHI), i.e., solar radiation scattered by clouds and particles in the atmosphere. These radiation comes equally from all directions and θ is the angle of incidence of the beam.

A. Building Model and Training

We propose utilizing an ensemble learning approach for GHI prediction which may be utilized to build a more efficient energy resource allocation framework to power the FiWi network components. Ensemble learning is defined as a process by which multiple models are strategically generated and combined to solve a particular computational intelligence problem [33]. Ensemble learning is primarily used to get better predictive accuracy than achieved by each individual component model. The models that we chose to assess for the purpose of GHI prediction are: (a) Random Forest, (b) MLP, (c) CNN, and (d) Markov processes. The results for average predictions for 2019 is shown in Table II, where it can be observed that experimenting on dataset utilized for building the model for this work also indicated the random forest model to be most accurate, whereas the performance of Markov process is least accurate. Further, in terms of computational complexity, the random forest is a probabilistic method which builds multiple

decision trees with different subsets of the given feature set and finally aggregates the result from each decision tree to obtain the final result. Predicting a new data point using a trained random forest will execute operations at every level of each tree, resulting in $\mathcal{O}(n_{tree}k)$ run time complexity, where n_{tree} denotes the number of trees and k is the maximum depth of a tree within the forest [34]. A Multi-Layer Perceptron (MLP) is a neural network which contains an input and output layer with hidden layers in between. The resultant prediction complexity thus depends highly on the architecture of the network (number of hidden layers, number of features and the activation function). MLP prediction uses feature set of new data point and conduct matrix multiplications. Matrix multiplication of $\text{Matrix}_{i,j}$ and $\text{Matrix}_{j,k}$ in its most naïve form has the complexity of $\mathcal{O}(i * j * k)$. Additionally, the output will undergo an activation function which will conduct further operations on each layer. Since this operation has to be done every time the process moves from one layer to another, this will run $n - 1$ times where, n is the number of layers in the network. This complexity can be reduced via (a) utilizing different matrix multiplication algorithms and (b) parallelizing the process. Similarly, a CNN is an evolved version of a basic neural network that adds multiple convolution layers applied to the feature set to simplify and model an existing feature set. This is performed by identifying convolutional filters that are applied to the data using multiple dot products which are $\mathcal{O}(v)$ in complexity where v is the length of the vector being multiplied. This is followed by fully connected layers similar to a traditional neural network performing the same operations as detailed. Lastly, a Markov decision process is also a stochastic process which utilizes state transitions annotated with probabilities to identify the probability of an event occurring. Assigning a complexity is challenging to a Markov process due to its stochastic nature as well as the desired termination criteria. In addition to this, for the purposes of our experiment, the utilization of Markov processes delivered fairly inaccurate results (as can be seen in Table II) and thus are not apt for prediction problems of this nature.

TABLE II
SOLAR IRRADIANCE PREDICTION FOR THE YEAR 2019

Model	Accuracy
Random forest	87.1%
Deep learning (MLP)	50.49%
Deep learning(CNN)	58.33%
Markov process	50%

A random forest regression ensemble learning model, consisting of multiple decision trees is selected for GHI prediction in this work, which along with all the advantages of ensemble learning additionally is known to combat overfitting, which individual decision trees are prone to, and thus providing strong predictive performance [35]. This type of model has previously been utilized for prediction of solar irradiance profile and is found to be most accurate when compared to

other regression models, namely support vector machine and linear regression [36].

In random forest, each decision tree is build using a random sample of data point drawn without replacement [37]. Decision trees learn how to best split the data set into smaller and smaller subsets to predict the target value [37]. There are various algorithms to implement a decision tree, however, we have used classification and regression trees (CART) algorithm as it supports numerical target variables or regressions [38]. CART constructs binary trees using feature and a threshold that yields the largest information gain (IG) and minimum MSE at each node. MSE is computed as follows [39]:

$$\text{MSE} = \frac{1}{N} \sum (x_a - x_p)^2, \quad (6)$$

where x_a is the actual value, x_p is the predicted value, and N denotes the total samples.

The predictions from all the decision trees are pooled to make the final prediction, i.e., the mean of all the predictions is calculated to get the output of random forest regression.

B. Data Set

The data set containing measured irradiance data as well as features such as year, month, day, hour, minute, temperature, dew point, DHI, DNI, GHI, ozone, relative humidity, solar zenith angle, surface albedo, pressure, precipitable water, and wind speed from the years 2001-2014 and 2017-2019 from [28] is available for the purposes of predictive model building. After feature engineering, we used the following features of the data set: day, hour, temperature, dew point, relative humidity, solar zenith angle, pressure, and precipitable water. The model is trained on the training set containing data available from years 2001-2018 and tested on the data for 2019². The irradiance data for 2015 and 2016 is not available at NREL [28], therefore we used the data for other years. Fig. 4 shows the solar irradiance profile for New Delhi for a set of 7 days of the prediction year 2019. It can be seen that the maximum irradiance is 620 W/m². Further, it is also evident that the day-to-day correlation of solar irradiance is insignificant.

For building ML model to predict the GHI value, we segregate the yearly data into 12 parts, one for each month of the year. For each month, the model is trained with the same month of the prior years, i.e., from 2001-2014 and 2017-2018. For instance, if the data for Jan-2019 is to be predicted, the model is trained with January 2001-2014 and 2017-2018. Further, as the solar zenith angle has the maximum information gain of 0.482, hence it is chosen as the first attribute for the split. The number of estimators in the GHI predictive model is 1000, i.e., there are 1000 trees in each forest, and the prediction value is calculated based on the mean of the outputs of these estimators.

²As proof of concept we are illustrating the performance for New Delhi, India, however the results will be applicable to other cities as well.

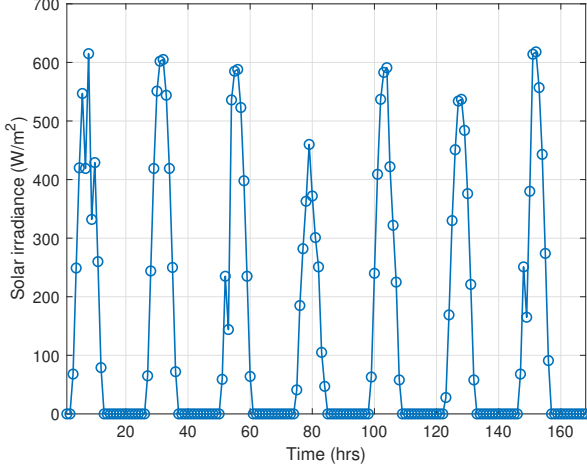


Fig. 4. GHI for a set of 7 days of 2019 for New Delhi.

C. Testing

To evaluate the performance of solar irradiance prediction, we use the following performance metrics: a) R^2 score, b) RMSE, and c) %RMSE. These metrics are described in detail below:

1) R^2 score: R^2 score is a statistical measure in a regression model that determines the proportion of variance of the dependent variable, where the dependent variable is defined by an independent variable. In other words, R^2 shows how well the data fits into the regression model, i.e., the goodness of fit. R^2 is calculated as [40]:

$$R^2_{score} = 1 - \left(\frac{\sum (x_a - x_p)^2}{\sum (x_a - x_{mean})^2} \right), \quad (7)$$

where x_a is ground truth, x_p is predicted value and x_{mean} is mean of all the actual values.

2) RMSE: Root Mean Squared Error is the measure of differences between values predicted by the model. In other words, it is standard deviation of the prediction errors and is calculated by [40]:

$$RMSE = \sqrt{\frac{1}{N} \sum (x_a - x_p)^2}. \quad (8)$$

3) %RMSE: It refers to the percentage RMSE and is calculated as [39]:

$$\%RMSE = \frac{\text{Calculated RMSE}}{\text{Maximum value of prediction}} \times 100. \quad (9)$$

IV. PROBLEM FORMULATION

In this section, a joint energy resource optimization problem to minimize the number of batteries as well as the number of PV panels required to operate ONU-AP is formulated. It is worthwhile to mention that the number of batteries depends on the number of PV panels and vice-versa. This is due to the fact that power of the PV panels is required to charge the batteries completely at T^{th} hour. Similarly, the number of the batteries depends on the power required by ONU-AP during

the non-solar hours. The optimization problem thus formulated is given as:

$$(P1) \quad \min_{N_P, N_B, B_{CHG}^1} C_P N_P + C_B N_B, \quad (10)$$

$$s.t. \quad \beta P_{B_{cap}} \leq B_{CHG}^1(t) \leq P_{B_{cap}}, \quad \forall t \in [0, 23], \quad (11)$$

$$P_{B_{cap}} \leq B_{CHG}^1(T), \quad (12)$$

$$N_P P_S^1(t) + N_B B_{CHG}^1(t) \geq P_O(t), \quad \forall t \in [0, 23]. \quad (13)$$

where N_P and N_B is the number of PV panels and batteries, respectively, and $N_P, N_B \in \mathbb{Z}$. C_P and C_B is the cost of PV panels and batteries, respectively. $P_{B_{cap}}$ is the battery capacity of the single battery, β is the depth of discharge value of the battery, $B_{CHG}^1(t)$ is the charge of a single battery at t^{th} hour, $P_S^1(t)$ is the power of a solar panel at t^{th} hour, and $P_O(t)$ is the power consumption of ONU-AP at t^{th} hour. The solar power $P_S^1(t)$ is calculated using (3), where the irradiance profile is calculated using ML based prediction. The optimization problem (10) minimizes the cost of required number of PV panels and batteries, i.e., $C_P N_P$ and $C_B N_B$, respectively by finding the optimal values of number of PV panels (N_P) and number of batteries (N_B). The constraint in (11) depicts that the charge of each battery at t^{th} hour, $B_{CHG}^1(t)$ does not exceed $P_{B_{cap}}$ and does not discharge below the depth of discharge $\beta P_{B_{cap}}$, i.e., $P_{B_{cap}} \in [\beta P_{B_{cap}}, P_{B_{cap}}], \forall t \in [0, 23]$. The second constraint in (12) denotes that the battery should be completely charged at the T^{th} hour. The power of ONU-AP should be fulfilled at each hour, i.e., the sum of power of the PV panel and batteries, $N_P \times P_S^1(t) + N_B \times B_{CHG}^1(t)$ must fulfill the power requirement of ONU-AP, $P_O(t) \forall t \in [0, 23]$.

As evident in (10), the cost of a PV panel and battery, is given by, C_P and C_B , respectively. The cost of PV panel includes the asset cost, C_{P_A} and operation and management (O&M) cost of the PV panel, C_{P_O} [41]:

$$C_P = C_{P_A} + C_{P_O}. \quad (14)$$

Similar to the cost of PV panel, the cost of a battery is calculated as [41]

$$C_B = C_{B_A} (N_R + 1) + C_{B_O}, \quad (15)$$

where C_{B_A} is 'the asset cost of the battery, C_{B_O} is the operation and management cost of a battery, N_R is the number of times the batteries are replaced within a system lifetime duration.

It is evident from (10) that the objective function is a linear function of optimization variables N_P and N_B . However, the constraint in (13) is quadratic in nature as it contains multiplication of two unknown variables N_B and $B_{CHG}^1(t)$. Hence, the optimization problem (P1) is a quadratic constraint linear programming problem (QCLP) [42]. This can be solved by sub-dividing the above problem into two sub-problems and solve them alternatively to get the final energy resource allocation. In [43], the authors provided an efficient algorithm based on an alternating solution scheme which alternates between solving a deterministic alternating current (AC) optimal power flow problem and assessing the impact of uncertainty. The

authors claimed that the flexibility of the alternating scheme enables not only scalable implementations, but also alternating chance-constraint reformulations. The authors compared the solutions obtained when solving the AC chance constrained optimal power flow either as a one-shot optimization problem and using an alternating solution algorithm. The results showed that the alternating algorithm provides optimal results. The authors in [44] proposed an alternating approach of using Pontryagin's minimum principle, namely alt-PMP for developing optimal energy management strategies for battery/supercapacitor hybrid energy storage systems. The authors compared the proposed solution with dynamic programming (DP) in terms of both computational efficiency and accuracy. The proposed alternating method performs superior to DP as numerical computations are required only for boundary conditions and for the constraints. The authors further mentioned that the proposed method can provide an effective tool for energy management strategy developers to use as an optimal benchmark to evaluate their real-time sub-optimal strategies. Thus, we have used alternating approach where each sub-problem is then solved alternatively to calculate the required energy resources allocation. The two sub-problem are given as follows:

A. Minimum PV panel allocation for a fixed number of batteries (MinPVAlloc)

This subsection proposes a PV panel allocation algorithm to allocate minimum number of PV panels required to operate ONU-AP for a fixed number of batteries. Let the fixed number of batteries be N_{B_F} , then the minimum number of PV panels required to charge the batteries and operate ONU-AP is calculated as shown in Algorithm 1.

Initialize the number of PV panels to N_P . As we know that the batteries should be entirely charged at T^{th} hour, thus we iterate the algorithm till $B_{CHG}(T + 24)$ is equal to the capacity of N_{B_F} batteries, $P_{B_{cap}}^N = N_{B_F} \times P_{B_{cap}}$. At each hour, t , calculate the amount of solar power allocated to ONU-AP, $P_{SO}(t)$ is given by:

$$P_{SO}(t) = \min\{P_O(t), \alpha P_S(t)\}, \quad \forall t \in [0, 23], \quad (16)$$

where $P_O(t)$ is the power consumption of ONU-AP and $\alpha P_S(t)$ is the fraction of solar power supplied to ONU-AP. As we know that the battery is charged by the fraction of solar power supplied to the battery, $(1 - \alpha)P_S(t)$ and the battery power at each hour is given by:

$$B_{CHG}(t) = \min\{B_{CHG}(t) + (1 - \alpha)P_S(t), P_{B_{cap}}^N\}. \quad (17)$$

If the solar power supplied to ONU-AP ($\alpha P_S(t)$) at t^{th} hour is less than the power required by ONU-AP ($P_O(t)$) then, the power will be consumed from the batteries. The power consumed from the batteries is given by:

$$P_{DIS}(t) = \max\{P_O(t) - P_{SO}(t), 0\}. \quad (18)$$

In case the fraction of power supplied to ONU-AP is higher than the solar power required by ONU-AP, then the excess solar power at ONU-AP is calculated as:

$$P_{EX}(t) = \max\{\alpha P_S(t) - P_{SO}(t), 0\}. \quad (19)$$

Further, at the beginning of next hour, we calculate the state of the battery using $P_{EX}(t)$, $P_{DIS}(t)$, $B_{CHG}(t)$.

$$B_{CHG}(t + 1) = \begin{cases} \beta P_{B_{cap}}^N, & B_{CHG}(t) - P_{DIS}(t) + P_{EX}(t) < \beta P_{B_{cap}}^N \\ \min\{B_{CHG}(t) - P_{DIS}(t) + P_{EX}(t), P_{B_{cap}}^N\}, & \text{otherwise} \end{cases} \quad (20)$$

Finally, the minimum number of PV panels is calculated based on the number of PV panels required to charge the fixed number of batteries at T^{th} hour. The complexity of Algorithm 1 is calculated as: $\mathcal{O}(24 \times Count_{PV}) = \mathcal{O}(Count_{PV})$, where $Count_{PV}$ is the minimum number of batteries required to power ONU-AP and $\mathcal{O}(\cdot)$ is the Big O notation that gives an asymptotic upper bound on a function as defined in [45].

Algorithm 1 MinPVAlloc Algorithm

Input:

N_{B_F} = Fixed number of batteries

Initialize:

$B_{CHG}(T) = N_{B_F} \times P_{B_{cap}}$

$N_P = 1$

$P_{B_{cap}}^N = N_{B_F} \times P_{B_{cap}}$

```

1: while  $B_{CHG}(T + 24) = P_{B_{cap}}^N$  do
2:   for  $t = T$  to  $T + 23$  do
3:      $P_{SO}(t) = \min\{P_O(t), \alpha P_S(t)\}$ 
4:      $B_{CHG} = \min\{B_{CHG}(t) + (1 - \alpha)P_S(t), P_{B_{cap}}^N\}$ 
5:      $P_{DIS}(t) = \max\{P_O(t) - P_{SO}(t), 0\}$ 
6:      $P_{EX}(t) = \max\{\alpha P_S(t) - P_{SO}(t), 0\}$ 
7:     if  $B_{CHG}(t) - P_{DIS}(t) + P_{EX}(t) < \beta P_{B_{cap}}^N$  then
8:        $B_{CHG}(t + 1) = \beta P_{B_{cap}}^N$ 
9:     else
10:       $B_{CHG}(t + 1) =$ 
11:         $\min\{B_{CHG}(t) - P_{DIS}(t) + P_{EX}(t), P_{B_{cap}}^N\}$ 
12:    end if
13:  end for
14:   $N_P = N_P + 1$ 
15: end while

```

Output: N_P is the minimum PV panels allocated to ONU-AP for N_{B_F} batteries.

B. Minimum battery allocation for a fixed number of PV panels (MinBatAlloc)

In Algorithm 2, we propose a battery allocation algorithm to allocate the minimum number of batteries required to operate ONU-AP. The input to the algorithm is a fixed number of PV panels, N_{P_F} . The minimum number of batteries required to operate ONU-AP during the non-solar hours is calculated as follows: Let us initialize the number of batteries to $N_B = 1$. For each iteration, the value of N_B is increased by 1 till

Algorithm 2 *MinBatAlloc* Algorithm

Input: N_{P_F} = Fixed number of PV panels**Initialize:** $B_{\text{CHG}}(T) = P_{B_{\text{cap}}}$ $P_{\text{out}} = 1 \times 24$ vector with all values = 1 $N_B = 1$ $P_S^M = N_{P_F} \times P_S^1$

```
1: while  $\sum_{t=0}^{23} P_{\text{out}}(t) = 0$  do
2:   for  $t = T$  to  $T + 23$  do
3:      $P_{\text{SO}}(t) = \min\{P_{\text{O}}(t), \alpha P_{\text{S}}(t)\}$ 
4:      $B_{\text{CHG}} = \min\{B_{\text{CHG}}(t) + (1 - \alpha)P_{\text{S}}(t), P_{B_{\text{cap}}}\}$ 
5:      $P_{\text{DIS}}(t) = \max\{P_{\text{O}}(t) - P_{\text{SO}}(t), 0\}$ 
6:      $P_{\text{EX}}(t) = \max\{\alpha P_{\text{S}}(t) - P_{\text{SO}}(t), 0\}$ 
7:     if  $B_{\text{CHG}}(t - 1) - P_{\text{DIS}}(t) + P_{\text{EX}}(t) < \beta P_{B_{\text{cap}}}$  then
8:        $P_a(t) = 1$ 
9:        $B_{\text{CHG}}(t + 1) = \beta P_{B_{\text{cap}}}$ 
10:    else
11:       $P_a(t) = 0$ 
12:       $B_{\text{CHG}}(t + 1) = \min\{B_{\text{CHG}}(t) - P_{\text{DIS}}(t) + P_{\text{EX}}(t), P_{B_{\text{cap}}}\}$ 
13:    end if
14:  end for
15:   $N_B = N_B + 1$ 
16: end while
```

Output: N_B is the minimum batteries allocated to ONU-AP for N_{P_F} PV panels.

the power outage, i.e., the amount of time the power is not available to ONU-AP is equal to zero. The solar power allocated to ONU-AP is given as follows:

$$P_{\text{SO}}(t) = \min\{P_{\text{O}}(t), \alpha P_{\text{S}}(t)\}, \quad (21)$$

where $P_{\text{O}}(t)$ is the power consumption of ONU-AP and $\alpha P_{\text{S}}(t)$ is the fraction of solar power supplied to ONU-AP. The fraction of solar power supplied to the batteries $(1 - \alpha)P_{\text{S}}(t)$ will charge the batteries and the battery power at each hour is given by $B_{\text{CHG}}(t)$:

$$B_{\text{CHG}}(t) = \min\{B_{\text{CHG}}(t) + (1 - \alpha)P_{\text{S}}(t), P_{B_{\text{cap}}}\}. \quad (22)$$

Further, if the solar power available to ONU-AP is insufficient to operate ONU-AP, then the power will be consumed from the batteries. The power consumed from the batteries is given by:

$$P_{\text{DIS}}(t) = \max\{P_{\text{O}}(t) - P_{\text{SO}}(t), 0\}. \quad (23)$$

Moreover, the excess solar at ONU-AP, that is, the power remaining after power requirement of ONU-AP is satisfied is supplied to charge the batteries. This excess power is given as:

$$P_{\text{EX}}(t) = \max\{\alpha P_{\text{S}}(t) - P_{\text{SO}}(t), 0\}. \quad (24)$$

Further, we calculate the battery state at the beginning of next hour using $B_{\text{CHG}}(t + 1)$, which is given by:

$$B_{\text{CHG}}(t + 1) = \begin{cases} \beta P_{B_{\text{cap}}}^N, & B_{\text{CHG}}(t) - P_{\text{DIS}}(t) + P_{\text{EX}}(t) < \beta P_{B_{\text{cap}}}^N \\ \min\{B_{\text{CHG}}(t) - P_{\text{DIS}}(t) + P_{\text{EX}}(t), P_{B_{\text{cap}}}^N\}, & \text{otherwise} \end{cases} \quad (25)$$

Further, for the hours where the charge in the batteries goes below the depth of discharge value, $\beta P_{B_{\text{cap}}}$, we calculate the power outage which is given by:

$$P_{\text{out}}(t) = \begin{cases} 0, & B_{\text{CHG}}(t) - P_{\text{DIS}}(t) + P_{\text{EX}}(t) < \beta P_{B_{\text{cap}}} \\ 1, & \text{otherwise.} \end{cases} \quad (26)$$

Finally, the minimum the number of batteries for which $\sum_{t=0}^{23} P_{\text{out}}(t) = 0$ can be computed. The complexity of Algorithm 2 can be calculated as $\mathcal{O}(24 \times \text{Count}_B) = \mathcal{O}(\text{Count}_B)$.

V. PERFORMANCE EVALUATION

In order to validate the performance of the proposed *MERA*, we compare the following approaches of energy resource allocation:

- 1) **Maximum energy resource allocation (*Max* approach):** In this approach, the energy resource allocation is calculated based on the worst solar power profile, i.e., lowest 24-hour solar power profile of the year. In this approach, the energy resources allocated are generally under-utilized, i.e., the energy resources allocated are much higher compared to the required energy resources. However, using this approach the probability of power outage is low.
- 2) **Minimum energy resource allocation (*Min* approach):** In this approach, the energy resource allocation is calculated based on the best solar power profile, i.e., highest 24-hour solar power profile of the year. For instance, in [46], the authors used peak power to optimally place PV panels in distribution network. Generally, this approach allocates minimum energy resources, and therefore, system might not be able to operate the device at all hours and suffer from severe power outage.
- 3) **Median energy resource allocation (*Median* approach):** In this approach, the energy resource allocation is calculated based on the median 24-hour solar power profile of the year, i.e., the median of all 365 days of the year.
- 4) **Outage threshold based energy resource allocation:** If the tolerable power outage limit predefined by the operator as $\Gamma\%$ outage per year then, based on $\Gamma\%$ outage, the energy resources required to operate ONU-AP are calculated. We have considered the outage threshold $\Gamma = 2\%$ which has been suggested in [47].
- 5) **Proposed ML based dynamic energy resource allocation (*MERA*):** In this approach, dynamic energy resource allocation is facilitated based on the solar power profile for each day. As we know that the number of batteries (PV panels) required by ONU-AP vary for each day based on the solar power profile of each day; therefore, the

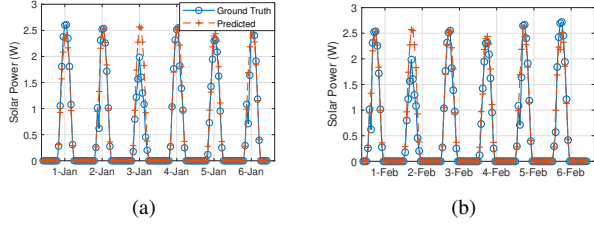


Fig. 5. Actual vs. Predicted solar power profile for New Delhi for first six days of a) January 2019 and b) February 2019.

energy resources should be dynamically allocated based on ONU-AP's requirement and solar power availability. The advantage of this approach is that the unutilized batteries will not be charged or discharged during the day, and hence, it will affect the performance of the system, which is discussed in detail in Section VI.

VI. RESULTS

The performance of the proposed joint energy resource allocation framework for the FiWi network is shown in this section. As mentioned before, in order to allocate the required number of batteries and PV panels to operate ONU-AP a joint energy resource allocation is used. Further, the proposed approach is compared with the other approaches of energy resource optimization such as *Max*, *Min*, *Median*, and outage threshold approach assuming both with wind and without wind scenarios. Moreover, the time at which the batteries are entirely charged is considered to be $T = 16:00$ hours. The DoD value for the battery, β is considered to be 0.7 [1]. The capacity of the single PV panel and battery is considered to be 5W [48], [49].

TABLE III
 R^2 SCORES FOR DIFFERENT MONTHS

Month	R^2 score	Month	R^2 score
January	91.00%	July	71.00%
February	83.15%	August	79.71%
March	86.53%	September	84.20%
April	93.24%	October	95.00%
May	93.96%	November	85.07%
June	84.64%	December	65.00%
Year			84.375%

A. Efficiency of machine learning predictions

The solar irradiance predictions for New Delhi for January and February 2019 are analyzed in this section. Fig. 5 shows the predictions of GHI for New Delhi for the first six days of January and February of 2019. It can be seen for each month the prediction is close to the actual values of solar irradiance. As mentioned before, in order to validate the predictions we calculate R^2 score, RMSE and % RMSE for the predicted solar irradiance values. The R^2 scores are presented in Table III. It can be seen that the average R^2 score for the year is 84.375%. For October, the R^2 score is the highest, i.e., the prediction for October is most accurate. However, for the months of

TABLE IV
 R^2 SCORES FOR DIFFERENT MONTHS OF 2018

Month	R^2 score	Month	R^2 score
January	83.76%	July	77.57%
February	91.87%	August	82.81%
March	91.43%	September	73.19%
April	92.35%	October	96.28%
May	92.46%	November	95.18%
June	85.78%	December	94.00%
Year			84.375%

TABLE V
RMSE SCORES FOR DIFFERENT MONTHS OF 2019

Month	RMSE	% RMSE	Month	RMSE	% RMSE
January	82.71	9.19	July	104.79	11.64
February	92.54	10.28	August	96.42	10.71
March	87.00	9.67	September	85.97	9.55
April	81.87	9.09	October	70.97	7.8
May	80.26	8.91	November	79.08	8.78
June	93.74	10.41	December	150.74	16.74
Year		92.17%			10.23%

July, August, and December, the prediction is least accurate as R^2 score is low³. In order to find out whether the trend for these months is similar to other years, we predicted the solar irradiance for 2018 by using 2017's data as the testing set. The results for R^2 score for 2018 are summarized in Table IV. GHI predictions for July and August continued to be least accurate when predicting for the year 2018 by training on data before the year 2017, however the model is able to predict GHI for the month of December as successfully as the other months [$R^2 = 94.00\%$] indicating that perhaps the month of December in 2019 is anomalous.

The RMSE values for different months of 2019 are shown in Table V. It can be observed that RMSE for October is the lowest, i.e., 7.8%, which is also aligned with the R^2 score for October is the highest. Further, for December, the RMSE is the highest, i.e., 150.74. Moreover, the average %RMSE for 2019 is 10.23%.

B. Energy resource allocation

In this subsection, we analyze the energy resources required to operate ONU-AP. The joint optimization problem ($P1$) is solved using an alternating approach, where the required number of batteries and PV panels are calculated alternatively until convergence. It may be noted that the proposed algorithm converges when the required number of batteries (or PV panels) at the current iteration and previous iteration are the same, i.e., $x(k+1) = x(k)$, where x is the number of batteries (or PV panels) and k is the number of iterations at which the algorithm converges. For iterative approach, the convergence happens at third iteration, where the number of batteries and PV panels converges as shown in Fig. 6. It is evident that

³The reason for July, August, and December to have lowest score might be due to rainy season. The solar irradiance is unpredictable in the rainy weather, while this does not apply for the month of December as it is winter season in New Delhi.

for the first iteration, the number of PV panels and batteries are the highest, while as the number of iterations increases, the required number of batteries and PV panels converges. Fig. 7 shows the variation of the number of batteries and PV panels required to operate ONU-AP with the variation of α . It is evident that the energy resources required for without wind scenario are more compared to with wind scenario. This is due to the fact that with the addition of wind energy, the dependency of ONU-AP on PV panels and batteries reduces, therefore, the number of batteries and PV panels required are also lower. Moreover, as the number of batteries is dependent on the power consumption of ONU-AP during the non-solar hour, thus the number of batteries is not affected by change in α . Furthermore, it can also be observed that as the fraction of

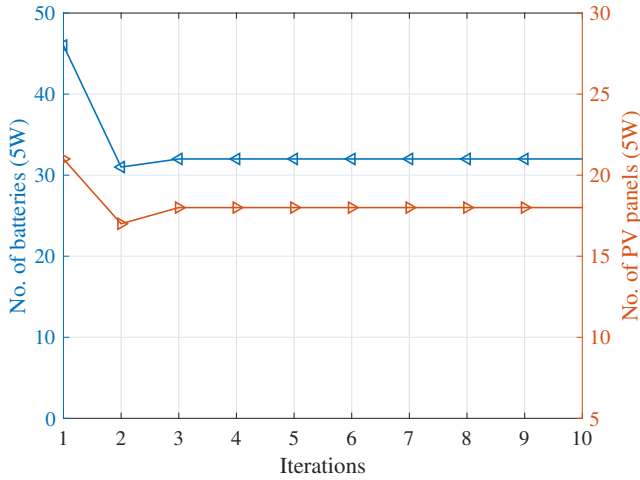


Fig. 6. Convergence of the proposed approach for New Delhi for without wind scenario.

solar power allocated to ONU-AP increases, i.e., α increases, the number of PV panels required by ONU-AP decreases. Moreover, with the increase in α from 0.2 to 1, there is a

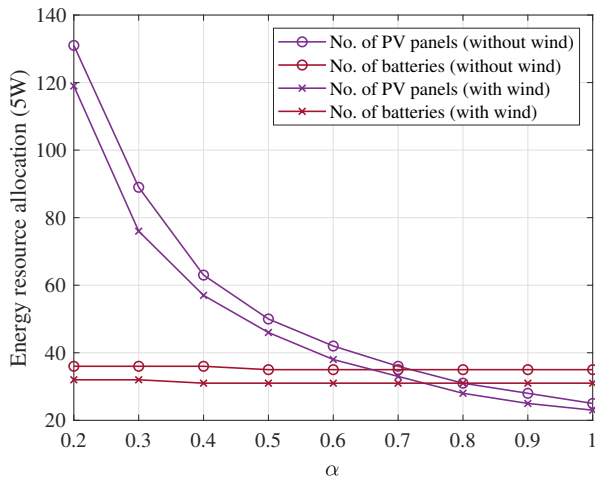
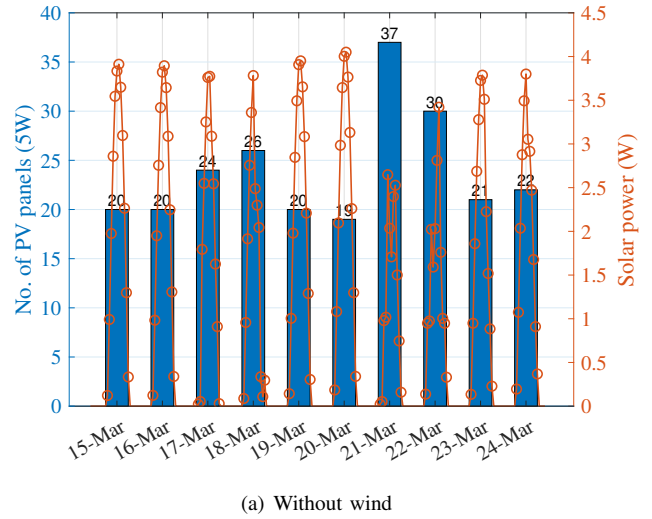
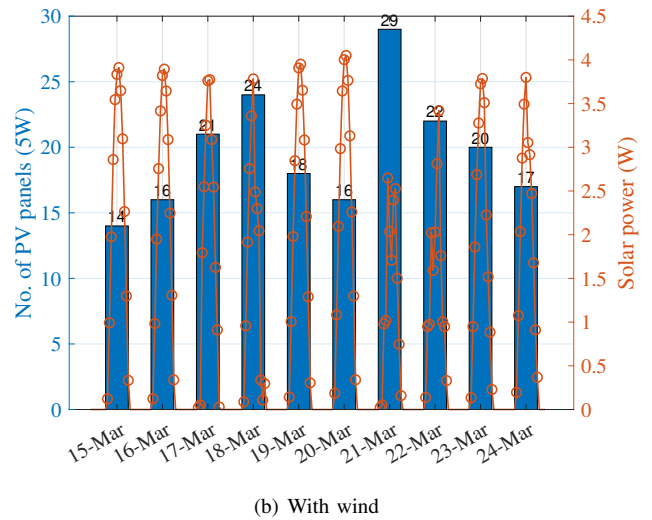


Fig. 7. Energy resource allocation with variation of α



(a) Without wind



(b) With wind

Fig. 8. PV panel allocation according to solar profile.

reduction in the number of PV panels from 130 to 24 for without wind scenario. Similarly, there is a reduction in the number of PV panels from 120 to 22 for with wind scenario.

In Fig. 8, the PV panel allocation from 15-Mar-2019 to 24-Mar-2019 is shown. It is evident from Fig. 8(a) that as the solar power for 21th March is the least thus, the number of PV panels required by ONU-AP is the highest, i.e., 37 for without wind scenario and 29 for with wind scenario. Similarly, the solar power for 20th March is the highest; thus, the number of PV panels for this day is 19. If we use wind energy, then the number of PV panels reduces by 3. Further, it is observed that for with wind scenario the number of PV panels not only depends on the solar power but also depend on the wind power. Hence, the required number of PV panels is smaller for 15th March as compared to 20th March.

The amount of energy resources required by ONU-AP for different approaches is shown in Fig. 9. It is evident that with *Min* approach the energy resource allocated to ONU-

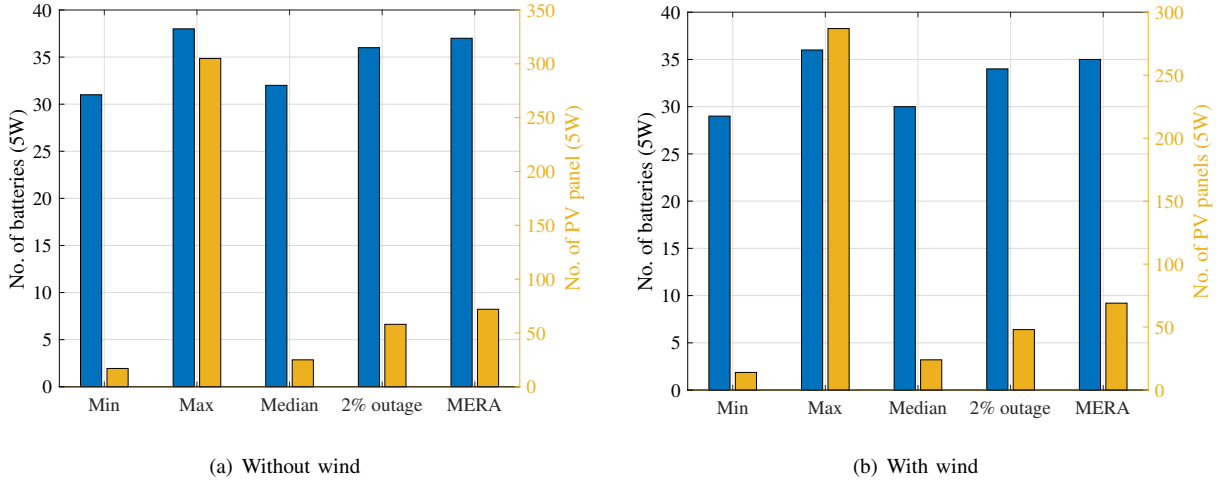


Fig. 9. The number of batteries (blue bars) and PV panels (yellow bars) required by ONU-AP for i) Approach I: *Min* approach, ii) Approach II: *Max* approach, iii) Approach III: *Median* approach, iv) Approach IV: *2% outage* approach, v) Approach III: Proposed *MERA*.

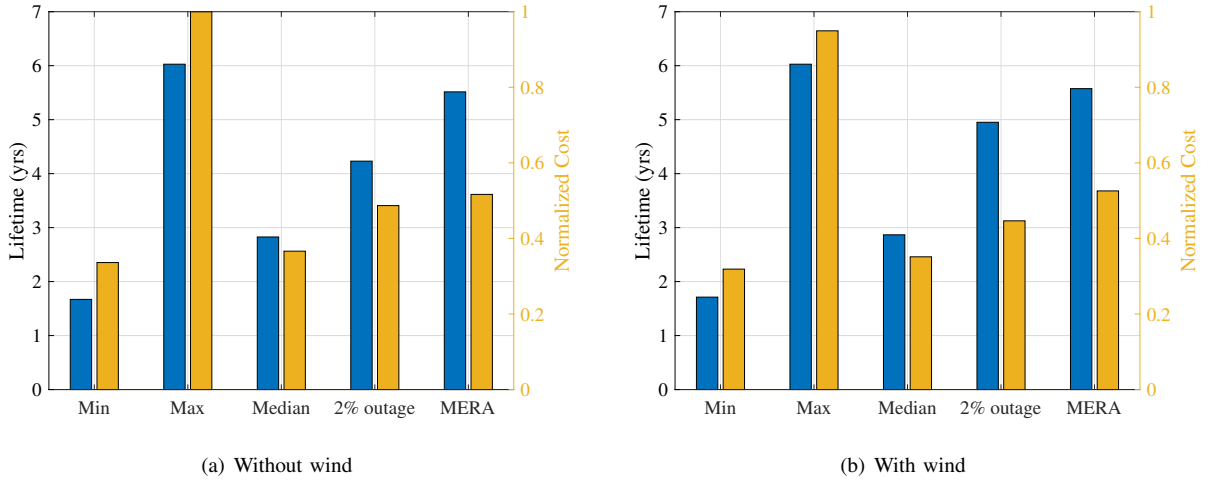


Fig. 10. Battery lifetime (blue bars) and normalized cost (yellow bars) analysis for New Delhi at 40 Mbps throughput for i) Approach I: *Min* approach, ii) Approach II: *Max* approach, iii) Approach III: *Median* approach, iv) Approach IV: *2% outage* approach, and v) Approach V: Proposed *MERA*.

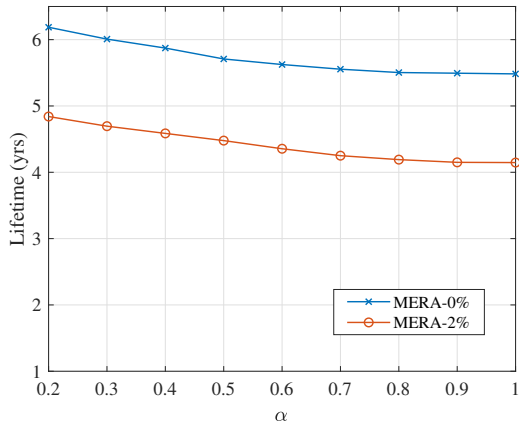


Fig. 11. Battery lifetime variation with respect to α

AP is lowest, while using *Max* approach the energy resource allocation is highest compared to other approaches followed by *MERA*, *2% outage*, *Median* and *Min* approach. Further, it is evident that there is a reduction of 235 PV panels and 1 battery using *MERA* compared to *Max* approach. For simulations, we have used the value of α to be 1, as the resource allocation for $\alpha = 1$ is the lowest. However, this will affect the lifetime of the batteries, which is analyzed in detail in later subsection. In order to alleviate the effect of energy resource allocation on battery lifetime, operator may choose the value of α such that the desired battery lifetime can be guaranteed.

C. Battery Lifetime

Battery lifetime of a lead-acid battery is dependent on the number of charging-discharging cycles of the battery. The number of charging discharging cycles are calculated

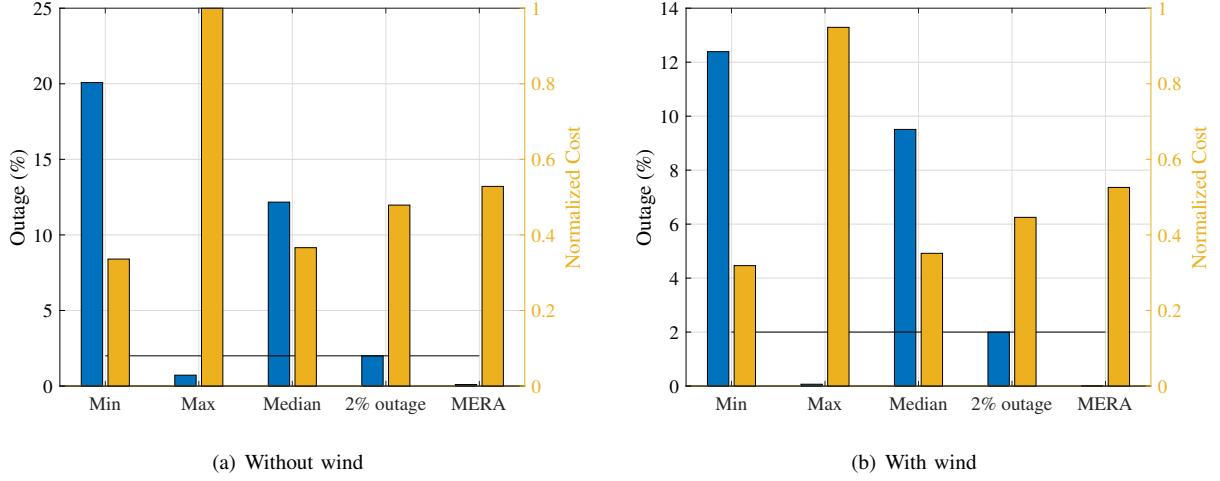


Fig. 12. Power outage (blue bars) and normalized cost (yellow bars) analysis for New Delhi at 40 Mbps throughput for i) Approach I: *Min* approach, ii) Approach II: *Max* approach, iii) Approach III: *Median* approach, iv) Approach IV: 2% outage approach, and v) Approach V: Proposed *MERA*.

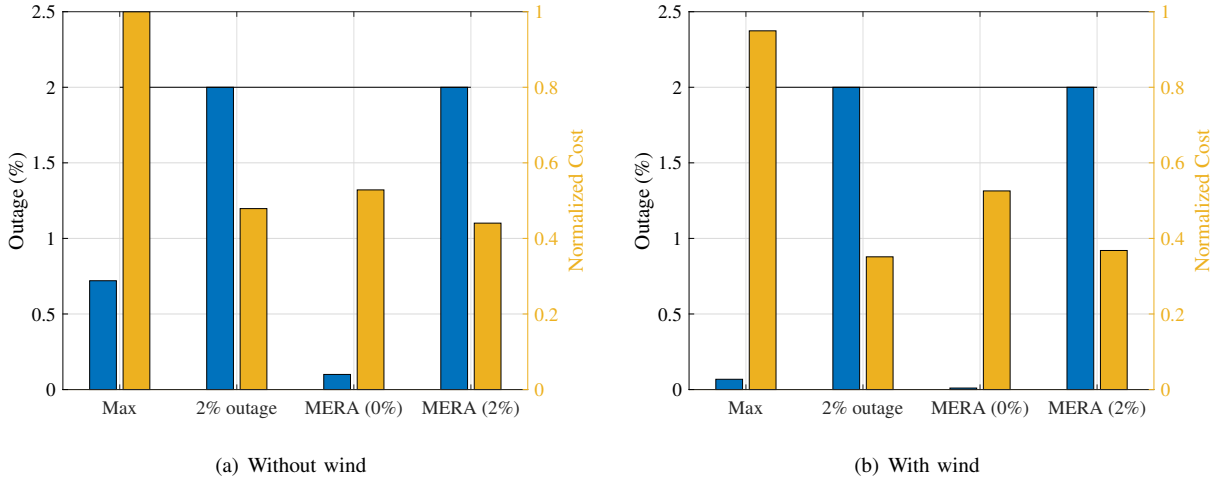


Fig. 13. Power outage (blue bars) and normalized cost (yellow bars) analysis for New Delhi at 40 Mbps throughput for the cases where outage is below the outage threshold of 2%, i.e., i) Approach I: *Max* approach, ii) Approach II: 2% outage approach, iii) Approach III: Proposed *MERA* with 0% outage and v) Approach IV: Proposed *MERA* allocation with 2% outage.

using rain-flow cycle counting algorithm [50]. A cycle to failure ratio (CTF_n) is specified by the operator based on the characteristic of the battery. The cycle to failure ratio represents the number of cycles the battery can have during its lifetime. The battery lifetime of a lead-acid battery can be calculated as follows [50]:

$$B_{lif} = \frac{1}{\sum_{n=1}^N \frac{C_n}{CTF_n}}, \quad (27)$$

where the number of cycles is denoted by C_n , CTF_n is the cycle to failure ratio, and the number of regions in which DoD is splitted is denoted by N .

Fig. 10 shows the lifetime and normalized cost analysis for the different approaches for with wind and without wind

scenarios. The cost of wind turbine is calculated as:

$$C_W = C_{W_A} + C_{W_O}, \quad (28)$$

where C_{W_A} is the asset cost of the wind turbine and C_{W_O} is the O&M cost of the wind turbine [41]. The asset and O&M cost of PV panel, battery, and wind turbine are summarized in Table VI. According to Table VI, the cost of battery can be calculated from (15). The lifetime of a battery is considered to be five years, and the lifetime of the PV panel and wind turbine is considered to be 20 years [41]. Further, we have considered the system lifetime to be equal to the lifetime of PV panel, and therefore, the total number of replacements of battery is three. Finally, the cost of 5W PV panel, battery and wind turbine are \$21.00, \$102.81, and \$17.60, respectively. The normalized cost of the system is calculated with respect

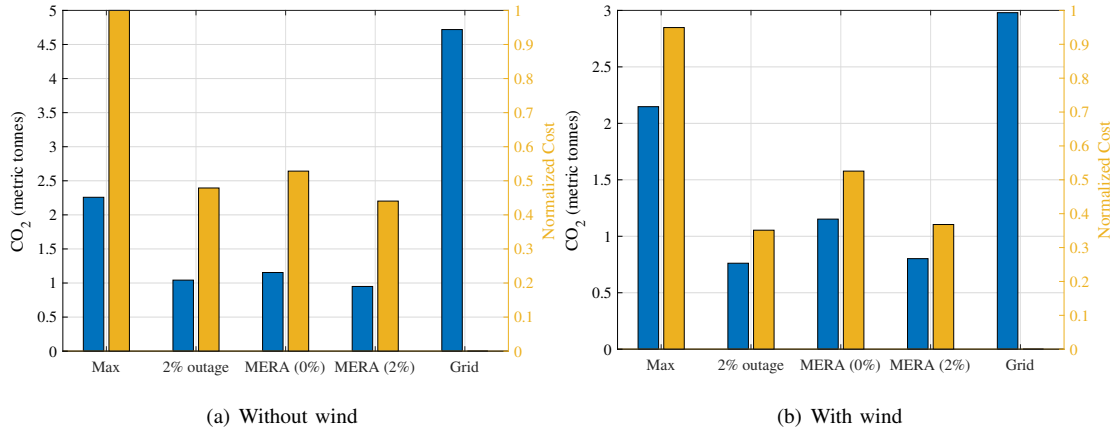


Fig. 14. CO₂ emissions (blue bars) and normalized cost (yellow bars) analysis for New Delhi at 40 Mbps throughput for i) Approach I: *Max* approach, ii) Approach II: 2% outage approach, iii) Approach III: Proposed *MERA* with 0% outage and v) Approach IV: Proposed *MERA* allocation with 2% outage.

TABLE VI
COST OF ENERGY RESOURCES [41]

Parameter	Values
Asset cost of battery	\$195/kWh
Asset cost of PV panel	\$3000/kWh
Asset cost of wind turbine	\$2500/kWh
O&M cost of battery	2% of C_B^{asset}
O&M cost of PV panels	2% of C_P^{asset}
O&M cost of wind turbine	2% of C_W^{asset}

to the cost of without wind scenario for *Max* approach. It is evident from Fig. 10 that as the normalized cost increases, the lifetime of the batteries increases. This is due to the fact that as the normalized cost increases, the energy resource allocation at the backup ONU-AP increases. With the increase in the number of batteries and PV panels, the batteries will discharge to a higher discharging value. As an example, for the same ONU-AP load, if the energy resource allocation is low, i.e., the number of batteries and PV panels allocated to operate ONU-AP is low. Then, the batteries will go to a lower discharge value in order to provide the same amount of power. Similarly, if the energy resource allocation is high, the batteries will not go to a lower discharge value. Thus, it can be seen from Fig. 10a, the *Min* approach has the least energy resource allocation, and therefore, the lifetime of the batteries is the least. Similarly, the *Max* approach has the highest cost as well as lifetime also. Further, the cost of *MERA* approach decreases by 67% however, the lifetime of the batteries decreases by only 10% compared to the *Max* approach, which is an advantage of *MERA*. While in comparison with the *Min*, *Median*, and 2% outage approaches, the battery lifetime is higher for the proposed algorithm. A similar trend in the lifetime of the proposed approach is seen in Fig. 10b for the with wind scenario where the lifetime of batteries decreases by 12% with a decrease in 67% of the cost for *MERA* approach as compared to *Max* approach.

In Fig. 11, the lifetime of the batteries with respect to α is

shown. It is evident that as α increases, the lifetime of the batteries decreases. This is because the energy resources allocated to ONU-AP decreases as α increases. As the allocated energy resources decreases, the batteries will have a lower state-of-charge or deep discharge. A battery of higher capacity might not discharge up to DoD limit, while a battery will lower capacity might have to go to deep discharge, and therefore, the lifetime of the battery decreases. Moreover, for *MERA* with 2% outage there is a further decrease in the energy resource allocation compared to *MERA* with 0% outage therefore, the lifetime of the batteries further decreases by 1 year 4 months for $\alpha = 1$.

D. Power outage analysis

This subsection analyzes the performance of the energy resource allocation framework in terms of power outage. The power outage in the system represents the amount of time (in %) for which the power supply to the ONU-AP is unavailable. It is evident from Fig. 12 that the outage for *MERA* approach is the least, while for *Min* approach the outage is maximum. Further, it is evident that for *Min*, *Max*, *Median*, and 2% outage approach, the outage is inversely proportional to the normalized cost. As the normalized cost increases, the outage decreases. This is due to the fact that as the normalized cost increases, the energy resource allocation also increases, thus the probability that power will not be available to ONU-AP is less and the outage will decrease. Moreover, the advantage of the proposed *MERA* in terms of outage is clearly evident from Fig. 12a. The outage for *MERA* is 0% which 0.5% less than the outage from *Max* approach, whereas in terms of cost a reduction of 67% is achieved. A similar trend is achieved for with wind scenario in Fig. 12b, where the outage for proposed *MERA* is the least. Further, it can be seen from Fig. 12 there are only three approaches providing outage less than the considered operator's power outage threshold of 2%. These three approaches are compared with the proposed *MERA* with 2% outage in Fig. 13 for without and with wind scenario.

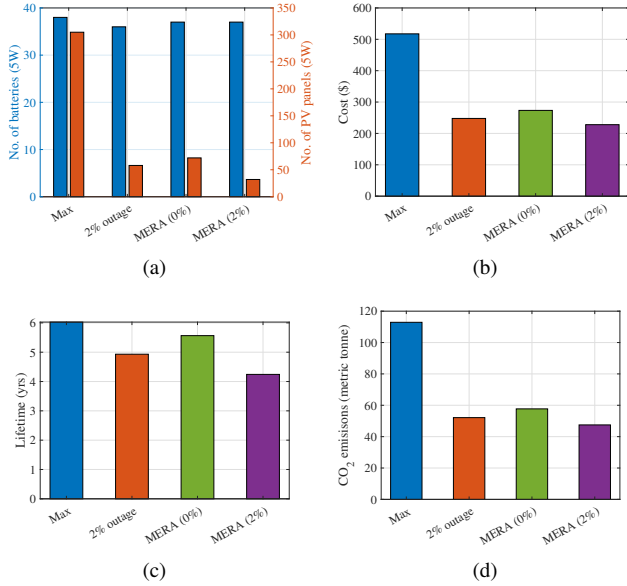


Fig. 15. Analysis for (a) Energy resource allocation, (b) Cost, (c) Lifetime, and (d) CO₂ emissions for different approaches for without wind scenario.

It is evident that *MERA* with 2% outage has a lower energy resource requirement compared to the other three approaches. If we compare two approaches with equal outage, i.e., *MERA* with 2% outage and 2% outage with non-ML based energy resource allocation, it is evident that using *MERA* the energy resource requirement is less. Moreover, there is a trade-off between *MERA* with 2% and *MERA* with 0% outage, i.e., as normalized cost increases, the outage decreases.

E. Carbon footprint analysis

The environmental impact of the energy resource allocation scheme in terms of CO₂ emissions is shown in Fig. 14. The CO₂ emissions for battery, wind turbine, and PV panel are 4.22, 0.96, and 0.96 tonnes CO₂/MWh, respectively [51]. For 2017-18, the weighted average CO₂ emission for India is 0.82 tCO₂/MWh [52]. It can be observed from Fig. 14 that the CO₂ emissions for FiWi network are proportional to the allocated energy resources. This is due to the fact that as the amount of energy resource increases, the cost and CO₂ emissions from the energy resources increases. Further, it is evident from Fig. 14 that CO₂ emissions as well as cost is the least for *MERA* with 2% outage, which is 63% and 73% lesser than the grid power supply for without and with wind scenario, respectively.

F. Trade-off analysis between energy resource allocation, battery lifetime, power outage, cost, and CO₂ emissions

The trade-off between energy resource allocation, battery lifetime, power outage, cost, and CO₂ emissions is shown in Fig. 15. In comparison with *Max* energy resource allocation, i.e., the best case scenario, there is a reduction of 235 PV panels and 2 batteries compared to *MERA* with 0% outage. Similarly, a reduction in cost of \$200, 0.5% outage, and

47.82% CO₂ emissions is evident for *MERA* with 0% outage compared to *Max* approach. However, there is a decrease in lifetime by 6 months compared to *Max* approach. Thus, a trade off between lifetime and energy resource allocation is clearly evident from Fig. 15. Further, in comparison with ML based 2% outage scheme, the energy resource requirement of *MERA* with 0% outage increases by 10%, however, the lifetime of the batteries decreases by 18% with a decrease in outage of 2%. Furthermore, for the same outage of 2%, the advantage of *MERA* compared to non-ML based 2% outage scheme is evident in terms of reduction in the number of PV panels by 30, the number of batteries by 1, 21.47% cost, and 18.64% CO₂ emissions. However, as there is a trade-off between lifetime and energy resource allocation, thus, with the use of *MERA* there is a reduction in lifetime of batteries by 6 months (10%). However, it can be noted that with the reduction in lifetime by 10%, there is an improvement in CO₂ emissions and cost by 21.47% and 18.64%, respectively. Thus, it can be concluded that using *MERA* the performance of the system is improved.

VII. CONCLUSIONS

In this paper, we proposed a joint energy resource optimization framework to minimize the batteries and PV panels required to operate ONU-AP for a FiWi network. We divided the optimization problem into two sub-problems: 1) Minimum PV panel allocation for a fixed number of batteries (*MinBatAlloc*) and 2) Minimum battery allocation for a fixed number of PV panels (*MinPVAlloc*). These two sub-problems are then solved alternatively to calculate the energy resources required by ONU-AP for with and without wind scenario. Further, in order to classify the fraction of solar power supplied to operate ONU-AP and battery we introduced a system parameter α and analyzed its impact on system performance such as, energy resource allocation and lifetime. Moreover, we compared the performance of our proposed approach *MERA* with the non-ML based approaches, such as *Max*, *Min*, *Median*, and outage threshold. The results showed that using *MERA* there is a reduction in energy resource allocation, cost, CO₂ emissions as well as outage compared to *Max* energy resource allocation, which is the best case scenario. However, in comparison to *Max* resource allocation, there is a reduction of battery lifetime by 10%. Thus, a trade-off between energy resource allocation and lifetime has been shown in this paper. Moreover, for the same outage limit of 2%, the proposed *MERA* has a reduction in 18.64% CO₂ emissions, 21.47% cost, 30 PV panels, and 1 battery in comparison of *MERA* with 0% outage. However, due to the reduction in energy resources, there is a decrease in battery lifetime of 10% for *MERA* with 0% outage compared to *MERA* with 2% outage. The possible future extension of the proposed work can be study of different throughput profiles and propose a scheme where the trade-off between energy resource allocation and lifetime can be further minimized.

VIII. ACKNOWLEDGEMENT

We would like to thank Dr. Arunima Srivastava, Ph.D. (The Ohio State University) for her valuable contributions towards the machine learning modeling aspects of this work.

REFERENCES

- [1] A. Gupta, A. Srivastava, and V. A. Bohara, "Resource allocation in solar-powered FiWi networks," *IEEE Access*, vol. 8, pp. 198 691–198 705, 2020.
- [2] "Global energy review 2021," 2021. [Online]. Available: <https://www.iea.org/reports/global-energy-review-2021/renewables>
- [3] "IDC - Global ICT spending: Forecast 2020 – 2023," 2020. [Online]. Available: <https://www.idc.com/promo/global-ict-spending/forecast>
- [4] B.-k. Jeon and E.-J. Kim, "The energy and carbon footprint of the Global ICT and E&M sectors 2010–2015," *Sustainability*, 2018.
- [5] S. Garg, A. Agrawal, S. Goyal, and K. Verma, "Day ahead solar irradiance forecasting using markov chain model," in *2020 IEEE 17th India Council International Conference (INDICON)*, 2020, pp. 1–5.
- [6] Y. Jiang, H. Long, Z. Zhang, and Z. Song, "Day-ahead prediction of bihourly solar radiance with a markov switch approach," *IEEE Transactions on Sustainable Energy*, vol. 8, no. 4, pp. 1536–1547, 2017.
- [7] M. Abuella and B. Chowdhury, "Solar power forecasting using artificial neural networks," in *2015 North American Power Symposium (NAPS)*, 2015, pp. 1–5.
- [8] Q. Liu and Q.-J. Zhang, "Accuracy improvement of energy prediction for solar-energy-powered embedded systems," *IEEE Transactions on Very Large Scale Integration (VLSI) Systems*, vol. 24, no. 6, pp. 2062–2074, 2016.
- [9] B.-k. Jeon and E.-J. Kim, "Next-day prediction of hourly solar irradiance using local weather forecasts and LSTM trained with non-local data," *Energies*, vol. 13, no. 20, 2020.
- [10] M. Maier, "Fiber-wireless (FiWi) broadband access networks in an age of convergence: Past, present, and future," *Advances in Optics*, pp. 1–23, 2014.
- [11] M. Lévesque and M. Maier, "Probabilistic availability quantification of PON and WiMAX based FiWi access networks for future smart grid applications," *IEEE Transactions on Communications*, vol. 62, no. 6, pp. 1958–1969, 2014.
- [12] H. Zhang, Y. Hu, R. Wang, Z. Li, P. Zhang, and R. Xu, "Energy-efficient frame aggregation scheme in IoT over fiber-wireless networks," *IEEE Internet of Things Journal*, vol. 8, no. 13, pp. 10779–10791, 2021.
- [13] C. He, R. Wang, and Z. Tan, "Energy-aware collaborative computation offloading over mobile edge computation empowered fiber-wireless access networks," *IEEE Access*, vol. 8, pp. 24 662–24 674, 2020.
- [14] L. C. d. Souza, E. S. Lima, and A. C. S. Junior, "Implementation of a full optically-powered 5G NR fiber-wireless system," *IEEE Photonics Journal*, vol. 14, no. 1, pp. 1–8, 2022.
- [15] B. Yang, D. Wu, H. Wang, Y. Gao, and R. Wang, "Two-layer stackelberg game-based offloading strategy for mobile edge computing enhanced FiWi access networks," *IEEE Transactions on Green Communications and Networking*, vol. 5, no. 1, pp. 457–470, 2021.
- [16] X. Xu, J. Li, Y. Xu, Z. Xu, and C. S. Lai, "A two-stage game-theoretic method for residential PV panels planning considering energy sharing mechanism," *IEEE Transactions on Power Systems*, vol. 35, no. 5, pp. 3562–3573, 2020.
- [17] P. Chakraborty, E. Baeyens, P. P. Khargonekar, K. Poolla, and P. Varaiya, "Analysis of solar energy aggregation under various billing mechanisms," *IEEE Transactions on Smart Grid*, vol. 10, no. 4, pp. 4175–4187, 2019.
- [18] X. Li, L. Lyu, G. Geng, Q. Jiang, Y. Zhao, F. Ma, and M. Jin, "Power allocation strategy for battery energy storage system based on cluster switching," *IEEE Transactions on Industrial Electronics*, pp. 1–1, 2021.
- [19] S. Sekander, H. Tabassum, and E. Hossain, "Statistical performance modeling of solar and wind-powered UAV communications," *IEEE Transactions on Mobile Computing*, vol. 20, no. 8, pp. 2686–2700, 2021.
- [20] Q. Wen, X. He, Z. Lu, R. Streiter, and T. Otto, "A comprehensive review of miniaturized wind energy harvesters," *Nano Materials Science*, vol. 3, no. 2, pp. 170–185, 2021, nano Energy Materials and Devices for Miniaturized Electronics and Smart Systems. [Online]. Available: <https://www.sciencedirect.com/science/article/pii/S2589965121000180>
- [21] D. P. Van, B. P. Rimal, M. Maier, and L. Valcarengi, "ECO-FiWi: An energy conservation scheme for integrated fiber-wireless access networks," *IEEE Transactions on Wireless Communications*, vol. 15, no. 6, pp. 3979–3994, 2016.
- [22] N. E. X. Chu, W. Guo, and J. Zhang, "User data traffic analysis for 3G cellular networks," in *2013 8th International Conference on Communications and Networking in China (CHINACOM)*, 2013, pp. 468–472.
- [23] M. Theologou, M. Louta, G. Papadimitriou, and P. Sarigiannidis, "Analysing the optical network unit power consumption in the 10 GB-capable passive optical network systems," *IET Networks*, vol. 5, 02 2016.
- [24] A. Garcia-Saavedra, P. Serrano, A. Banchs, and G. Bianchi, "Energy consumption anatomy of 802.11 devices and its implication on modeling and design," in *Proceedings of the 8th International Conference on Emerging Networking Experiments and Technologies*, ser. CoNEXT '12. New York, NY, USA: Association for Computing Machinery, 2012, p. 169–180. [Online]. Available: <https://doi.org/10.1145/2413176.2413197>
- [25] L. Xue, L. Yi, H. Ji, P. Li, and W. Hu, "Symmetric 100-Gb/s TWDM-PON in O-band based on 10G-class optical devices enabled by dispersion-supported equalization," *Journal of Lightwave Technology*, vol. 36, no. 2, pp. 580–586, 2018.
- [26] C. B. Gaur, V. Gordienko, F. Bessin, and N. J. Doran, "Dual-band amplification of downstream L-band and upstream C-band signals by FOPA in extended reach PON," in *2020 European Conference on Optical Communications (ECOC)*, 2020, pp. 1–4.
- [27] "Push it to the limit! Understand Wi-Fi's breaking point to design better WLANs," 2015. [Online]. Available: <https://blogs.arubanetworks.com/industries/pushittohelimitunderstandwifisbreakingpointtodesignbetterwlan/>
- [28] "NSRDB: National solar radiation database." [Online]. Available: <https://nsrdb.nrel.gov/>
- [29] P. Gilman, "SAM photovoltaic model technical reference," 5 2015. [Online]. Available: <https://www.osti.gov/biblio/1215213>
- [30] J. Ouyang, M. Li, Z. Zhang, and T. Tang, "Multi-timescale active and reactive power-coordinated control of large-scale wind integrated power system for severe wind speed fluctuation," *IEEE Access*, vol. 7, pp. 51 201–51 210, 2019.
- [31] "NREL: System Advisor Model (SAM)." [Online]. Available: <https://sam.nrel.gov/>
- [32] J. Büngeler, E. Cattaneo, B. Riegel, and D. Sauer, "Advantages in energy efficiency of flooded lead-acid batteries when using partial state of charge operation," *Journal of Power Sources*, vol. 5, pp. 53–58, 01 2018.
- [33] R. Polikar, "Ensemble learning," *Scholarpedia*, vol. 4, no. 1, p. 2776, 2009, revision #186077.
- [34] X. Solé, A. Ramisa, and C. Torras, "Evaluation of random forests on large-scale classification problems using a bag-of-visual-words representation," vol. 269, pp. 273–276, 01 2014.
- [35] Z. Ma, J. Ma, Y. Miao, and X. Liu, "Privacy-preserving and high-accurate outsourced disease predictor on random forest," in *Information Sciences*, vol. 496, 2019, pp. 225–241.
- [36] Anuradha, K., Erlapally, Deekshitha, Karuna, G., Srilakshmi, V., and Adilakshmi, K., "Analysis of solar power generation forecasting using machine learning techniques," *E3S Web Conf.*, vol. 309, p. 01163, 2021. [Online]. Available: <https://doi.org/10.1051/e3sconf/202130901163>
- [37] A. Sharma, "Decision tree vs. random forest - which algorithm should you use?" 2020. [Online]. Available: <https://www.analyticsvidhya.com/blog/2020/05/decision-tree-vs-random-forest-algorithm/>
- [38] J. Lutes, "Entropy and information gain in decision trees," 2020. [Online]. Available: <https://towardsdatascience.com/entropy-and-information-gain-in-decision-trees-c7db67a3a293>
- [39] S. Raschka, *Python Machine Learning*. Packt Publishing, 2015.
- [40] K. Srilakshmi and C. Sai Sruthi, "Prediction of TCS stock prices using deep learning models," in *2021 7th International Conference on Advanced Computing and Communication Systems (ICACCS)*, vol. 1, 2021, pp. 1448–1455.
- [41] R. Atia and N. Yamada, "Sizing and analysis of renewable energy and battery systems in residential microgrids," *IEEE Transactions on Smart Grid*, vol. 7, no. 3, pp. 1204–1213, 2016.
- [42] P. Gurram, H. Kwon, Z. Peng, and W. Yin, "Optimal sparse kernel learning for hyperspectral anomaly detection," in *2013 5th Workshop on Hyperspectral Image and Signal Processing: Evolution in Remote Sensing (WHISPERS)*, 2013, pp. 1–4.

- [43] L. Roald and G. Andersson, "Chance-constrained AC optimal power flow: Reformulations and efficient algorithms," *IEEE Transactions on Power Systems*, vol. 33, no. 3, pp. 2906–2918, 2018.
- [44] B.-H. Nguyen, T. Vo-Duy, M. C. Ta, and J. P. F. Trovão, "Optimal energy management of hybrid storage systems using an alternative approach of Pontryagin's minimum principle," *IEEE Transactions on Transportation Electrification*, vol. 7, no. 4, pp. 2224–2237, 2021.
- [45] T. H. Cormen, C. E. Leiserson, R. L. Rivest, and C. Stein, *Introduction to Algorithms*, 2nd ed. The MIT Press, 2001. [Online]. Available: <http://www.amazon.com/Introduction-Algorithms-Thomas-H-Cormen/dp/0262032937%3FSubscriptionId%3D13CT5CVB80YFWJEPWS02%26tag%3Dws%26linkCode%3Dxm2%26camp%3D2025%26creative%3D165953%26creativeASIN%3D0262032937>
- [46] R. Prenc, D. Škrlec, and V. Komen, "Optimal PV system placement in a distribution network on the basis of daily power consumption and production fluctuation," in *Eurocon 2013*, 2013, pp. 777–783.
- [47] "The Indian telecom services performance indicators October – December, 2020," 2021. [Online]. Available: https://www.trai.gov.in/sites/default/files/QPIR_27042021_0.pdf
- [48] Solar India 5 Watt 6 V Polycrystalline Solar Panel SS15 Watt. [Online]. Available: https://www.industrybuying.com/solar-panels-solar-india-SO.PO.1624861/?utm_source=Google&utm_medium=PLA&utm_campaign=PLA_New_Solar&gclid=CjwKCAjwxuuCBhATEiwAIIIz0cM4Smo1XsVvxLgq-dtdnkuTDZu_5hTLsX3IIJUvku4eVgdFvihZTRoC5ewQAvD_BwE
- [49] Hi Link HLK 5M12 12V/5W Switch Power Supply Module. [Online]. Available: https://robu.in/product/hlk-5m12-12v-5w-switch-power-supply-module/?gclid=CjwKCAjwxuuCBhATEiwAIIIz0ThdavQEYruvk7H3S55NoOYa5Dwk2\0acFmXX0p-2eNCpYwBYPLMYjRoCYvEQAvD_BwE
- [50] M. Alam and T. Saha, "Cycle-life degradation assessment of battery energy storage systems caused by solar PV variability," *IEEE Power and Energy Society General Meeting (PESGM)*, pp. 1–5, 07 2016.
- [51] D. Alder, A. Khodaei, and W. David Gao, "Standard measurement of carbon footprints," in *2016 North American Power Symposium (NAPS)*, 2016, pp. 1–5.
- [52] "CO₂ baseline database for the Indian power sector," 2018. [Online]. Available: https://cea.nic.in/wp-content/uploads/baseline/2020/07/user_guide_ver14.pdf